Supplementary methods

Patients' characteristics

Complete anamnestic data were recorded for all the patients, including age, patient weight and height, body mass index (BMI), previous abdominal operations, smoking status, Eastern Cooperative Oncology Group (ECOG) performance status, American Society of Anaesthesiologists (ASA) score, Charlson Comorbidity Index (CCI), history of hypertension and its treatment, history of acute myocardial infarction and its treatment, history of coronary artery disease and its treatment, history of peripheric vasculopathies, history of other comorbidities, presence of symptoms or sings at diagnosis, clinical tumor size, tumour location in the kidney, nephrometric scores (P.A.D.U.A. and R.E.N.A.L.) and TNM stage (according to 8th edition, 2017). Preoperative data were also recorded for all the patients, regarding preoperative imaging, cardiological evaluation, serum haemoglobin and creatinine levels, and complete blood count. Estimated glomerular filtration rate (EGFR) was calculated with the Chronic Kidney Disease Epidemiology Collaboration formula for younger patients (<70 years), and with the Berlin Initiative Study formula for older patients (≥70 years).

Histologic assessment

The following histological parameters were re-evaluated by an experienced and dedicated pathologist: tumour diameter, WHO/ISUP grade, histologic heterogeneity, presence of necrosis, of cystic component, of regions with a different WHO/ISUP grade and of lymphoid infiltration or aggregates.

Computed tomography acquisition protocol and image analysis

A 7 years experienced radiologist measured qualitative, semi-quantitative and quantitative radiological features from CT scan images obtained with a 64-slice multidetector CT scanner (Philips Brilliance 64, Philips, Best, The Netherlands). The CT protocol included scanning acquisition in four phases: unenhanced phase (UP), corticomedullary phase (CMP, at 30 seconds delay after contrast injection), nephrographic phase (NP, at 90 seconds delay after contrast injection) and excretory phases (EP, at 5 minutes delay after contrast injection).

The region of interest (ROI) was defined as the tumour area delimited in axal scan by use of a dedicated software (Intellispace portal v.8, Philips, Best, The Netherlands).

Central scar was defined as a central stellate hypoattenuating area in corticomedullary phase with a surface area lower than 5% than the scan area, with or without progressive enhancement in nephrographic phase. Pseudocapsule was defined as a high- or low-attenuation rim surrounding the tumor. Heterogeneity of the lesion was defined as the presence of different radiologic appearance. Calcification presence was also assessed.

Tumour enhancement was defined high if similar to renal cortex enhancement, moderate if similar to soft tissue enhancement but lower than renal cortex, low if slightly higher than water attenuation and with measurable contrast enhancement.

With regards to their attenuating pattern, both in the unenhanced and nephrographic phase, the lesions were defined as hypoattenuating, isoattenuating, hyperattenuating or mixed compared to adjacent parenchyma. Tumour composition (solid or cystic), necrosis and homogeneity [homogeneous (uniform in attenuation) or heterogeneous (mixed areas of attenuation)] were also assessed.

The following volumetric features were analysed: length of tumour in the short axis (measured in millimetres), length of tumour in the long axis (measured in millimetres); total tumour volume (measured in cubic centimetres); exophytic tumour volume (measured in cubic centimetres), and percentage of exophytic tumour volume.

The following features were analysed in UP images: mean, standard deviation, minimum and maximum tumour attenuation (measured in HU), attenuation of the psoas (measured in HU), the tumour-to-psoas attenuation ratio, calculated as the ratio between the maximum attenuating region of the tumour and the psoas attenuation; the tumour-to-kidney attenuation ratio, calculated as the ratio between the maximum attenuating region of the tumour and the renal cortex attenuation.

The following features were analysed on CMP images: mean, standard deviation, minimum and maximum tumour attenuation (measured in HU), the attenuation of the renal cortex (measured in HU), and tumour-to-kidney attenuation ratio.

 https://dx.doi.org/10.21037/tau-21-713

The following features were analysed on nephrographic phase (NP) images: mean, standard deviation, minimum and maximum tumour attenuation (measured in HU), the attenuation of the renal cortex (measured in HU), and tumour-to-kidney attenuation ratio.

The following enhancement features were also examined: (I) the early tumour enhancement (measured in HU), calculated as difference between the mean tumour attenuation in the CMP and the mean tumour attenuation in the UP, and (II) the late tumour enhancement (measured in HU), calculated as between the mean tumour attenuation in the NP and the mean tumour attenuation in the UP.

The following 19 features were selected for correlation analysis with transcriptomic signature:

(I) The mean attenuation of the tumour in unenhanced phase,
(II) The maximum attenuation of the tumour in the unenhanced phase,
(III) The minimum attenuation of the tumour in the unenhanced phase,
(IV) The attenuation of the renal cortex in the unenhanced phase,
(V) The tumour-to-psoas attenuation ratio in the unenhanced phase,
(VI) The tumour-to-kidney attenuation ratio in the unenhanced phase,
(VII) The mean attenuation of the tumour in the corticomedullary phase,
(VIII) The maximum attenuation of the tumour in the corticomedullary phase,
(IX) The minimum attenuation of the tumour in the corticomedullary phase,
(X) The attenuation of the renal cortex in the corticomedullary phase,
(XI) The tumour-to-kidney attenuation ratio in the corticomedullary phase,
(XII) The mean attenuation of the tumour in the nephrographic phase,
(XIII) The maximum attenuation of the tumour in the nephrographic phase,
(XIV) The minimum attenuation of the tumour in the nephrographic phase,
(XV) The attenuation of the renal cortex in the nephrographic phase,
(XVI) The tumour-to-kidney attenuation ratio in the nephrographic phase,
(XVII) The early tumour enhancement
(XVIII) The late tumour enhancement
(XIX) The attenuation of the psoas.

An example of 4 phase CT imaging is the showed in *Figure S1*.

Transcriptomics and RNA sequencing quality control

The tumoral molecular landscape was assessed through transcriptomic signature analysis. RNA sequencing was perfumed using quantseq 3' mrna-Seq library prep kit and the prepared libraries were sequenced on the Illumina nextseq 500 platform. Reads were generated towards a poly(A) tail.

Rnaseq quality control was performed by use of the multiqc v1.0. Dev0 (a4e3db2) platform (https://github.com/ewels/multiqc, developed by Phil Ewels et al., Science for Life Laboratory, Stockholm University, Stockholm 106 91, Sweden) (1) implementing the Bamtools toolkit to manage BAM files (http://github.com/pezmaster31/bamtools, developed by Derek Barnett et al., Marth Lab, Biology Dept., Boston College, Boston, USA) (2).

After calculation of Reads Per Kilobase of transcript per Million mapped reads (RPKM) values, the sequencing depth and the quality of alignment of the 6 samples were examined. Sequencing depth was found not to be high, with the reads being roughly between 3 and 5 million per sample. The majority of aligned genes are protein-coding genes. However, fractions of mitochondrial-ribosomal RNA (Mt_rrna), processed pseudogene and long intergenic noncoding RNAs (lincrna) were present (*Figure S2*).

The alignment quality, evaluated with the STAR ultrafast universal RNA-seq aligner plot (https://github.com/alexdobin/STAR developed by Alex Dobin et al., Cold Spring Harbor Laboratory, Cold Spring Harbor, NY, USA) (3), was good, with a high percentage of reads (around 80%) univocally mapped on the human genome (*Figure S3*).

The mean quality value across each base position in the read, measured by fastqc toolkit (developed by Simon Andrews et al., Babraham Bioinformatics, Babraham Institute, Cambridge, United Kingdom), was satisfactory as the Phred scored above 30 from base 1 to base 75 for each sample (*Figure S4*). The per sequence quality scores, measured through the fastqc toolkit,

 https://dx.doi.org/10.21037/tau-21-713

assessed the number of reads with average quality scores and suggested that no subset of reads had poor quality (*Figure S5*). Sequence duplication levels, measured by fastqc toolkit, by analysing the level of duplication found in each sequence, suggested that duplication levels were low: from 65.5% to 85% of the libraries in the different samples had no duplication (*Figure S6*). In addition, the total amount of overrepresented sequences found in each library, measured by fastqc toolkit, showed only 0.15% - 0.79% over-represented sequences in the different samples (*Figure S7*).

The data discussed in this publication have been deposited in NCBI's Gene Expression Omnibus and are accessible through GEO Series accession number GSE133460 (https://www.ncbi.nlm.nih.gov/geo/query/acc.cgi?Acc=GSE133460).

Statistical analysis

To assess the heterogeneity of the transcriptomes in the samples, Principal Component Analysis (PCA) was fitted. First, a PCA with all transcripts was performed. Then, a list of 369 out of 406 genes known to be associated with ccRCC from the 2013 Cancer Genome Atlas (TCGA) rnaseq and transcriptomic analysis was used (4), after excluding those genes with a constant expression in our samples in order to focus on transcripts really involved in ccRCC and avoid possible confounding (the list of the involved genes is below). A second PCA with this restricted list was performed, considering zero-centred RPKM values. While elaborating the ccRCC-associated gene list, we noted that 26 genes listed in the TGCA analysis were not referenced with the GENCODE basic annotation but with an alias, so a translation to the GENCODE basic annotation was made. Since PCA is unstable when the number of features is greater than the number of samples, we ran 1,000 re-sampling via bootstrapping. For each re-sampling the corresponding PCA was calculated and 50 genes with the highest loadings were obtained. Significant pathways in each Principal Components for these top 50 genes were assessed with Enrichr (Ma'ayan Laboratory, Computational Systems Biology, Mount Sinai Center for Bioinformatics, One Gustave L. Levy Place, Box 1603, New York, NY, USA), in relation to the KEGG 2016 database, while significant gene ontologies were assessed in relation to GO Cellular Component 2018, GO Biological Process 2018, and GO Molecular Function 2018, to evaluate respectively which pathways, cellular components, biological process, and molecular function impacted on the variance of the PC. Statistically significance was set at adjusted P value <0.05.

Pearson's correlation coefficients were used to assess correlation among 19 selected radiomic features themselves and between the radiomic features and RPKM values. Adjusted p-values were computed through Benjamini-Hochberg false discovery rate. Correlation was considered adequate if $\rho<-0.85$ or $\rho>0.85$.

To interpret the correlation data, a heatmap showing correlation between genes expression and radiomic features was drawn. A dendogram showed the hierarchical relationship between radiomic features and transcripts. Statistical significance of the radiogenomic correlation patterns was assessed with Mann-Whitney U test, for dichotomic comparison, or with Kruskal-Wallis tests, for multiple comparison. In order to obtain the graphics graphpad Prism (graphpad Software La Jolla, CA, USA) was used.

References

1. Ewels P, Magnusson M, Lundin S, et al. MultiQC: summarize analysis results for multiple tools and samples in a single report. Bioinformatics 2016;32:3047-8.
2. Barnett DW, Garrison EK, Quinlan AR, et al. BamTools: a C++ API and toolkit for analyzing and managing BAM files. Bioinformatics 2011;27:1691-2.
3. Dobin A, Davis CA, Schlesinger F, et al. STAR: ultrafast universal RNA-seq aligner. Bioinformatics 2013;29:15-21.
4. Creighton CJ, Morgan M, Gunaratne PH, et al. Comprehensive molecular characterization of clear cell renal cell carcinoma. Nature 2013;499:43-9.

 https://dx.doi.org/10.21037/tau-21-713

List of the 369 genes obtained from The Cancer Genome Atlas (TCGA) Rnaseq and transcriptomic analysis used for PCA

	Genes
1	*AGRN*
2	*CHD5*
3	*KIF1B*
4	*MTOR*
5	*CLCN6*
6	*VPS13D*
7	*SPEN*
8	*UBR4*
9	*ARID1A*
10	*CSMD2*
11	*ZMYM1*
12	*MACF1*
13	*USP24*
14	*PATJ*
15	*DOCK7*
16	*AGL*
17	*COL11A1*
18	*SLC16A4*
19	*LRIG2*
20	*ATP1A1*
21	*SPAG17*
22	*NOTCH2*
23	*PDE4DIP*
24	*NUP210L*
25	*ASH1L*
26	*GON4L*
27	*SPTA1*
28	*TNR*
29	*LAMC2*
30	*HMCN1*
31	*TPR*
32	*CFH*
33	*ASPM*
34	*CRB1*
35	*KIF14*
36	*KIF21B*
37	*NFASC*
38	*CR1*
39	*DNAH14*
40	*OBSCN*
41	*SIPA1L2*
42	*TARBP1*
43	*LYST*
44	*RYR2*
45	*PXDN*
46	*MYT1L*
47	*KIDINS220*
48	*GREB1*
49	*APOB*
50	*ITSN2*
51	*EMILIN1*
52	*CAD*
53	*BIRC6*
54	*PLEKHH2*
55	*LRPPRC*
56	*NRXN1*
57	*PAPOLG*
58	*USP34*
59	*XPO1*
60	*ALMS1*
61	*AFF3*
62	*GCC2*
63	*RANBP2*
64	*UGGT1*
65	*THSD7B*
66	*LRP1B*
67	*NEB*
68	*BAZ2B*
69	*SLC4A10*
70	*SCN1A*
71	*LRP2*

https://dx.doi.org/10.21037/tau-21-713

continued

	Genes
72	*NFE2L2*
73	*TTN*
74	*DNAH7*
75	*NDUFS1*
76	*ZDBF2*
77	*CPS1*
78	*ABCA12*
79	*FN1*
80	*ZFAND2B*
81	*DOCK10*
82	*SPHKAP*
83	*COL6A3*
84	*SETD5*
85	*VHL*
86	*SETD2*
87	*DOCK3*
88	*BAP1*
89	*PBRM1*
90	*USF3*
91	*ZBTB38*
92	*MED12L*
93	*ZBBX*
94	*PIK3CA*
95	*ATP13A4*
96	*BOD1L1*
97	*PCDH7*
98	*RFC1*
99	*KDR*
100	*ADGRL3*
101	*ANKRD17*
102	*FRAS1*
103	*WDFY3*
104	*PTPN13*
105	*TET2*
106	*NPNT*
107	*ANK2*

continued

continued

	Genes
108	*ANKRD50*
109	*FAT4*
110	*PCDH10*
111	*MAML3*
112	*DCHS2*
113	*FNIP2*
114	*RAPGEF2*
115	*TRAPPC11*
116	*FAT1*
117	*DNAH5*
118	*CDH18*
119	*PDZD2*
120	*ADAMTS12*
121	*NIPBL*
122	*MAST4*
123	*BDP1*
124	*CMYA5*
125	*VCAN*
126	*ADGRV1*
127	*DMXL1*
128	*SLC12A2*
129	*FBN2*
130	*RAPGEF6*
131	*RAD50*
132	*PCDHA12*
133	*PCDHB11*
134	*NSD1*
135	*FLT4*
136	*RREB1*
137	*HIVEP1*
138	*KIF13A*
139	*DNAH8*
140	*CUL9*
141	*ZNF318*
142	*XPO5*
143	*PKHD1*

continued

https://dx.doi.org/10.21037/tau-21-713

continued

	Genes
144	*DST*
145	*MDN1*
146	*LAMA2*
147	*UTRN*
148	*PPIL4*
149	*SYNE1*
150	*IGF2R*
151	*PLG*
152	*SDK1*
153	*ABCB5*
154	*DNAH11*
155	*HECW1*
156	*ABCA13*
157	*PCLO*
158	*AKAP9*
159	*COL1A2*
160	*RELN*
161	*CPED1*
162	*ZNF800*
163	*RBM28*
164	*KMT2C*
165	*CSMD1*
166	*CDCA2*
167	*NSD3*
168	*RP1*
169	*CHD7*
170	*ZFHX4*
171	*LRRCC1*
172	*VPS13B*
173	*ZFPM2*
174	*TG*
175	*PLEC*
176	*FREM1*
177	*GBA2*
178	*PRUNE2*
179	*COL15A1*

continued

continued

	Genes
180	*ABCA1*
181	*SVEP1*
182	*KIAA0368*
183	*RGS3*
184	*TNC*
185	*ODF2*
186	*LAMC3*
187	*CAMSAP1*
188	*DIP2C*
189	*FAM208B*
190	*FBXO18*
191	*UPF2*
192	*CUBN*
193	*MYO3A*
194	*ANK3*
195	*JMJD1C*
196	*DDX50*
197	*GRID1*
198	*PTEN*
199	*KIF20B*
200	*BTAF1*
201	*RRP12*
202	*GBF1*
203	*SMC3*
204	*SFXN4*
205	*MKI67*
206	*NAV2*
207	*CCDC73*
208	*KIAA1549L*
209	*TNKS1BP1*
210	*AHNAK*
211	*LRP5*
212	*PPFIA1*
213	*TENM4*
214	*SYTL2*
215	*FAT3*

continued

https://dx.doi.org/10.21037/tau-21-713

continued

	Genes
216	*BIRC2*
217	*DYNC2H1*
218	*ATM*
219	*EXPH5*
220	*CEP164*
221	*KMT2A*
222	*HSPA8*
223	*WNK1*
224	*CACNA1C*
225	*VWF*
226	*CHD4*
227	*PZP*
228	*GRIN2B*
229	*ABCC9*
230	*LRRK2*
231	*KMT2D*
232	*ACVR1B*
233	*ESPL1*
234	*ERBB3*
235	*LRP1*
236	*LRIG3*
237	*NAV3*
238	*NT5DC3*
239	*SART3*
240	*NOS1*
241	*GCN1*
242	*DNAH10*
243	*RIMBP2*
244	*ZMYM2*
245	*LATS2*
246	*SACS*
247	*PARP4*
248	*ATP8A2*
249	*MTUS2*
250	*BRCA2*
251	*NBEA*

continued

continued

	Genes
252	*FREM2*
253	*VWA8*
254	*MYCBP2*
255	*SLITRK6*
256	*NALCN*
257	*NYNRIN*
258	*ARHGAP5*
259	*RALGAPA1*
260	*TOGARAM1*
261	*SYNE2*
262	*PCNX1*
263	*YLPM1*
264	*FLRT2*
265	*AHNAK2*
266	*HERC2*
267	*RYR3*
268	*AQR*
269	*STARD9*
270	*FBN1*
271	*SECISBP2L*
272	*DMXL2*
273	*PRTG*
274	*VPS13C*
275	*HERC1*
276	*ITGA11*
277	*IL16*
278	*AKAP13*
279	*ACAN*
280	*ANPEP*
281	*IQGAP1*
282	*LRRK1*
283	*KIAA0430*
284	*MYH11*
285	*RBBP6*
286	*ZNF423*
287	*SALL1*

continued

continued

https://dx.doi.org/10.21037/tau-21-713

continued

	Genes
288	*CHD9*
289	*CNOT1*
290	*CDH8*
291	*CDH11*
292	*NFATC3*
293	*ZFHX3*
294	*ADAMTS18*
295	*ZC3H18*
296	*PRPF8*
297	*ZZEF1*
298	*POLR2A*
299	*TP53*
300	*DNAH2*
301	*CHD3*
302	*MYH13*
303	*NCOR1*
304	*MYO15A*
305	*SSH2*
306	*ATAD5*
307	*NF1*
308	*C17orf75*
309	*HEATR9*
310	*CDK12*
311	*NBR1*
312	*GPATCH8*
313	*KANSL1*
314	*MED13*
315	*SDK2*
316	*TTYH2*
317	*DNAH17*
318	*RNF213*
319	*LAMA1*
320	*ASXL3*
321	*SETBP1*
322	*LOXHD1*
323	*MYO5B*

continued

continued

	Genes
324	*ALPK2*
325	*CDH19*
326	*ZNF407*
327	*C3*
328	*FBN3*
329	*MUC16*
330	*COL5A3*
331	*SMARCA4*
332	*CACNA1A*
333	*ADGRE3*
334	*CPAMD8*
335	*TSHZ3*
336	*RYR1*
337	*SIGLEC8*
338	*PEG3*
339	*MACROD2*
340	*PHF20*
341	*PTPRT*
342	*NCOA3*
343	*PREX1*
344	*ARFGEF2*
345	*ZNFX1*
346	*SCAF4*
347	*SYNJ1*
348	*SON*
349	*BRWD1*
350	*PCNT*
351	*MICAL3*
352	*PI4KA*
353	*PRR14L*
354	*TRIOBP*
355	*EP300*
356	*TCF20*
357	*FBLN1*
358	*CELSR1*
359	*TUBGCP6*

continued

continued

https://dx.doi.org/10.21037/tau-21-713

continued

	Genes
360	*SBF1*
361	*DMD*
362	*HDAC6*
363	*KDM5C*
364	*HUWE1*
365	*TAF1*
366	*ATRX*
367	*COL4A5*
368	*STAG2*
369	*TENM1*

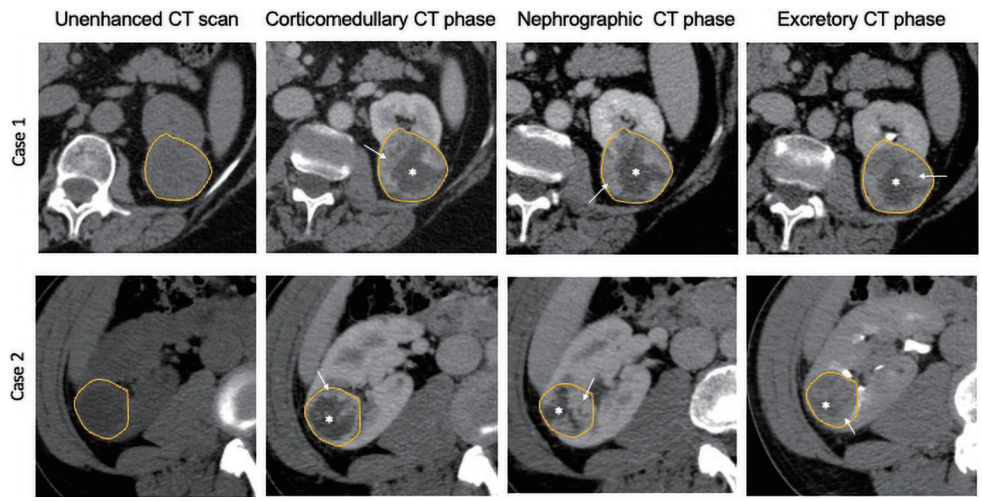

Figure S1 An example of 4 phase CT imaging is the following. Four-phase CT protocol (unenhanced, corticomedullary, nephrographic and excretory phases) in two cases of renal cell carcinoma (yellow ROIs in all images). Case 1 is a ccRCC of 4 cm diameter involving the upper third of the left kidney, Case 2 is a ccRCC of 3 cm involving the upper third of the right kidney. Both tumours showed similar features at qualitative assessment of each CT scan, being characterized by round shape, an hypervascular peripheral region (white arrows) and an irregular hypovascular central region (asterisks). At radiomic evaluation case 1 showed slightly lower HU in CMP and NP compared to case 2 (63 and 64 *vs.* 69 and 84 HU) but with higher maximum HU in both phases (168 and 139 HU *vs.* 120 and 106 HU) as for more necrotic lesion with higher degree of vascularization in the periphery. HU, Hounsfield Unit; CMP, corticomedullary phase; NP, nephrographic phase; ROI, Region Of Interest; ccRCC, clear cell Renal Cell Carcinoma; CT, Computed Tomography.

https://dx.doi.org/10.21037/tau-21-713

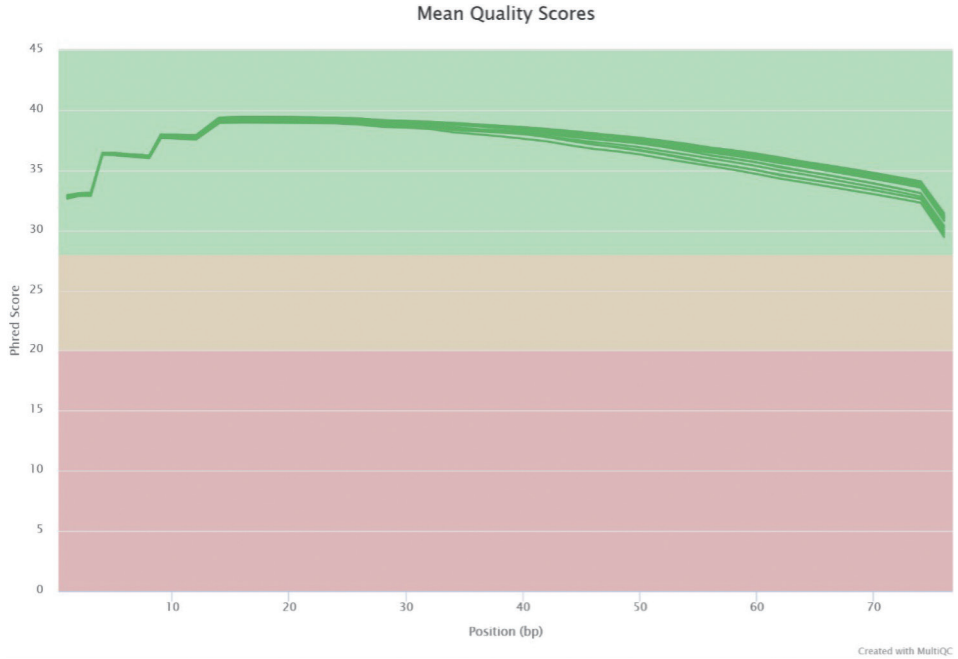

Figure S2 The mean quality value across each base position in the read was good, as the Phred scored remaining above 30 from base 1 to base 75 for each sample.

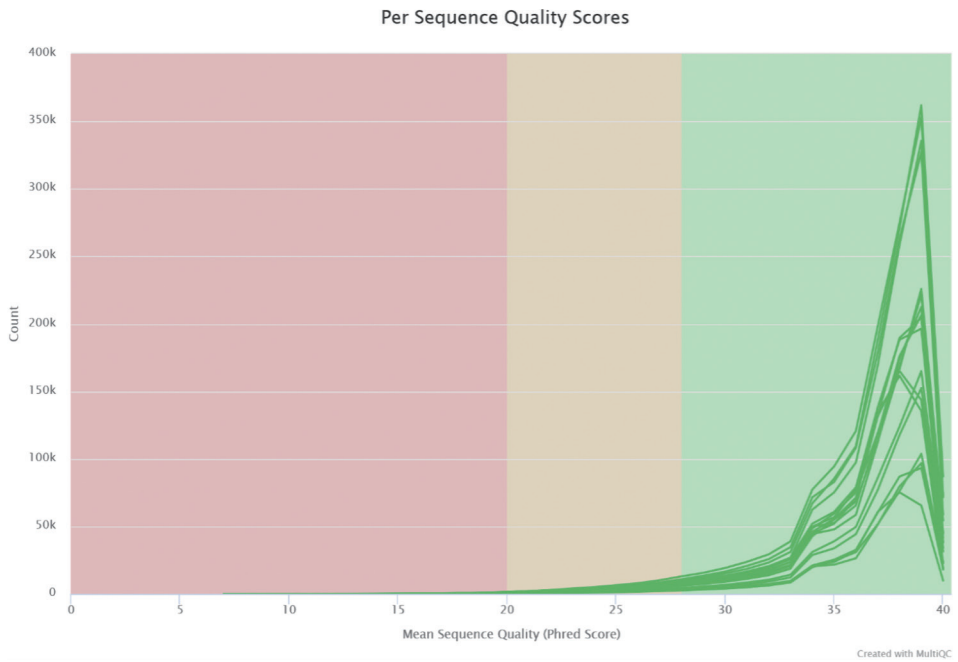

Figure S3 The per sequence quality scores, which evaluates the number of reads with average quality, suggested that no subset of reads has poor quality.

https://dx.doi.org/10.21037/tau-21-713

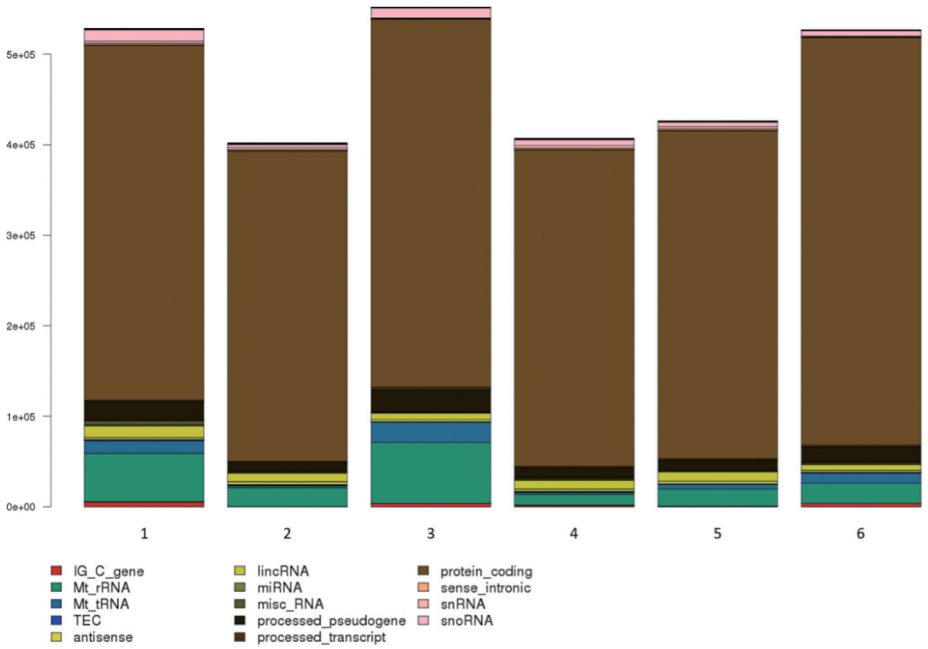

Figure S4 Biotypes distribution among samples, using RPKM values. 15935 expressed genes have been considered. IG_C_gene are Immunoglobulin (Ig) variable chain and T-cell receptor (tcr) genes imported or annotated according to IMGT (http://www.imgt.org/). Mt_rrna, Mt_trna, mirna, misc_RNA, snrna, snorna are non-coding RNA predicted using sequences from Rfam and mirbase (http://rfam.xfam.org/ & http://www.mirbase.org/). TEC are rnas that need to be experimentally validated, used for non-spliced EST clusters that have polya features; this category has been specifically created for the ENCODE project for regions that could indicate the presence of protein coding genes that require experimental validation. Antisense are transcripts that overlap the genomic span (i.e. Exon or introns) of a protein-coding locus on the opposite strand. LincRNA are long, intervening noncoding (linc) RNA that can be found in evolutionarily conserved, intergenic regions. Processed_pseudogene are pseudogenes that lack introns and are thought to arise from reverse transcription of mrna followed by reinsertion of DNA into the genome. Processed_transcript are transcripts not containing an open reading frame (ORF). Protein_coding are transcripts containing an ORF, thus thought to be protein coding. Sense_intronic are long non-coding transcript in introns of a coding gene that does not overlap any exons. RPKM, Reads Per Kilobase of transcript per Million mapped reads; Ig, Immunogolobuline; RNA, RiboNucleic Acid.

https://dx.doi.org/10.21037/tau-21-713

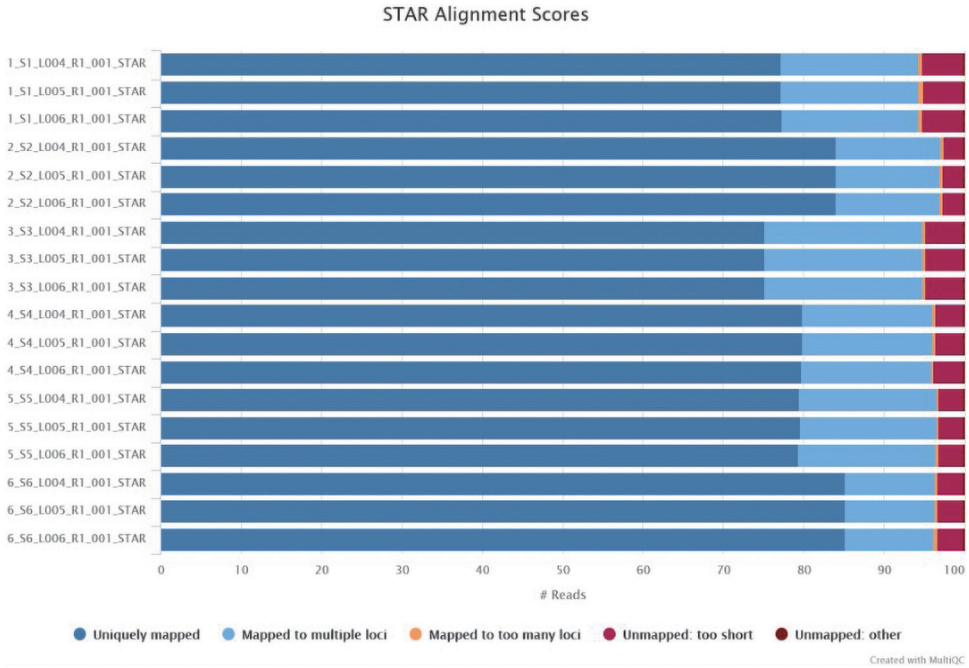

Figure S5 STAR alignment scores plot. RNA uniquely mapped ranges from 75.1% to 85.2%. RNA mapped to multiple loci ranged from 11% to 19.7%. RNA unmapped ranged from 2.6% to 5%.

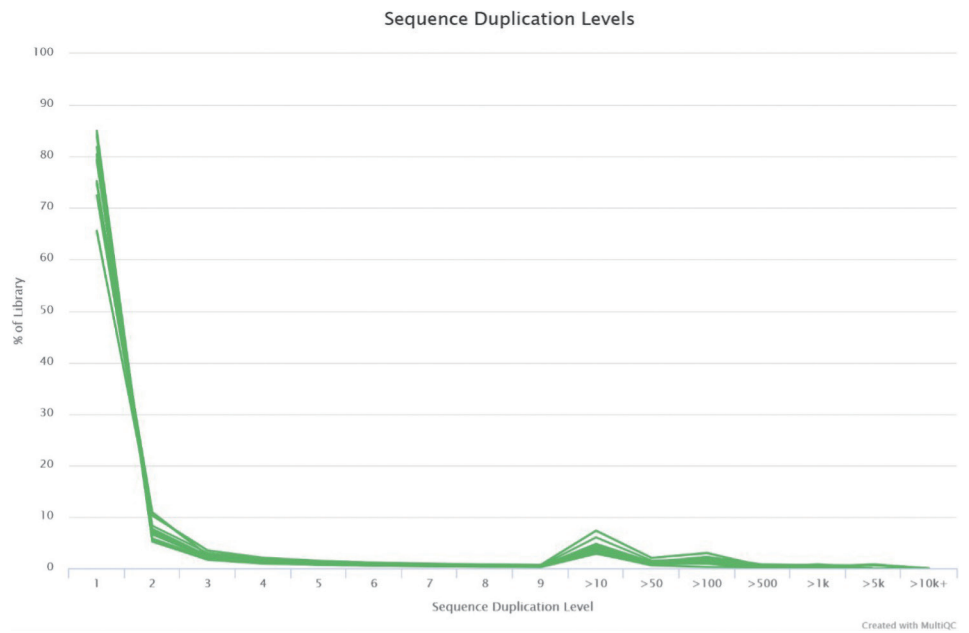

Figure S6 Sequence duplication levels, that show the relative level of duplication found in each sequence, were extremely low: from 65.5% to 85% of the libraries in the samples had no duplication.

https://dx.doi.org/10.21037/tau-21-713

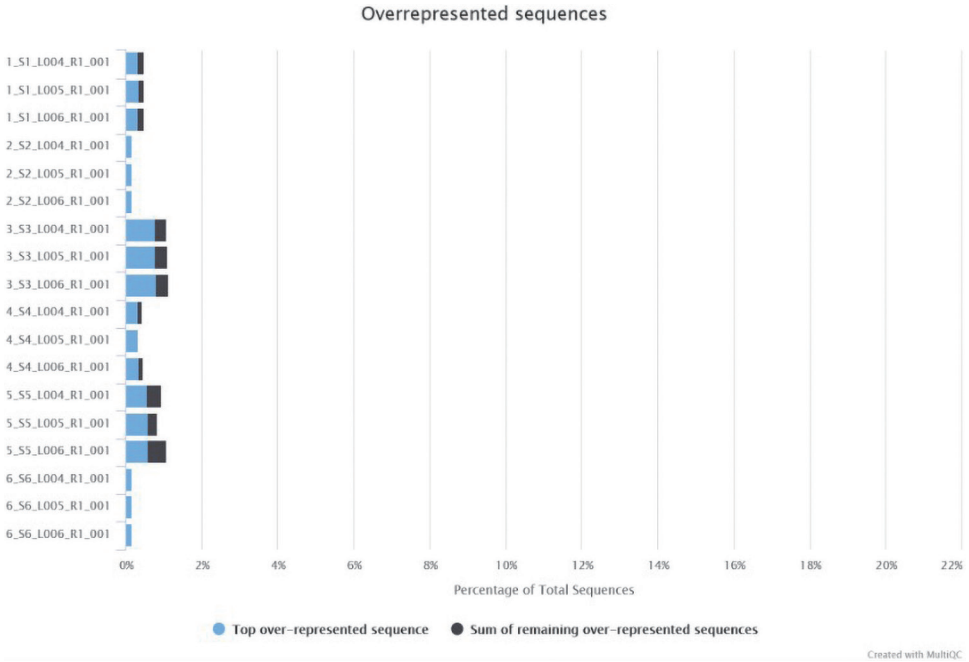

Figure S7 The graph shows the total amount of overrepresented sequences found in each library, with the top over-represented sequences ranging from 0.15% to 0.79% in the different samples.

https://dx.doi.org/10.21037/tau-21-713

Table S1 Radiomics characteristics at computed tomography imaging

Variable	
Volumetric data	
Long axis, mm	41 (32.5-46)
Short axis, mm	32 (30.5-41.5)
Total volume, cc	19.5 (16.2-38.4)
Exophytic volume, cc	12 (5-28.1)
Exophytic growth percentage, %	14.5 (13.1-15.6)
Unenhanced phase data	
Mean tumor attenuation, HU	25.5 (21-33.4)
Standard deviations tumor attenuation, HU	14 (11.8-19.3)
Maximum tumor attenuation, HU	35.6 (31.4-41.1)
Minimum tumor attenuation, HU	13 (9.8-27.8)
Psoas attenuation, HU	53.6 (50.6-59.6)
Tumor-to-Psoas ratio	0.67 (0.60-0.7)
Renal cortex attenuation, HU	31.3 (27.3-35.6)
Tumor-to-Kidney Ratio	1.22 (0.94-1.38)
Corticomedullary phase data	
Mean tumor attenuation, HU	133.9 (71.2-164.3)
Standard deviations tumor attenuation, HU	47.6 (32.2-67.7)
Maximum tumor attenuation, HU	168.3 (129.9-232.5)
Minimum tumor attenuation, HU	23.7 (14.7-65.4)
Renal cortex attenuation, HU	173 (155.5-204.8)
Tumor-to-Kidney Ratio	0.92 (0.81-1.19)
Nephrographic phase data	
Mean tumor attenuation, HU	97.9 (74.6-141.2)
Standard deviations tumor attenuation, HU	35.9 (27.5-44.3)
Maximum tumor attenuation, HU	139.4 (114.3-169.5)
Minimum tumor attenuation, HU	32.2 (17.2-74)
Renal cortex attenuation, HU	171 (146.7-241)
Tumor-to-Kidney Ratio	0.75 (0.69-0.81)
Enhancement data	
Early tumor enhancement	106.5 (50.2-131.9)
Late tumor enhancement	70.5 (53.6-108.7)

Four phases at CT scan were evaluated: unenhanced, i.e., before contrast injection; corticomedullary, i.e., 30 seconds after contrast injection; nephrographic, i.e., 90 seconds after contrast injection; excretory, i.e., 5 minutes after contrast injection. No data from the excretory phase were used for the analysis. Data are presented as median and interquartile range (IQR). HU, Hounsfield Units.

https://dx.doi.org/10.21037/tau-21-713